



Estimating real driving emissions from MAX-DOAS measurements at the A60 motorway near Mainz, Germany

Bianca Lauster¹, Steffen Dörner¹, Steffen Beirle¹, Sebastian Donner¹, Sergey Gromov¹, Katharina Uhlmannsiek¹, and Thomas Wagner¹

¹Max Planck Institute for Chemistry, Mainz, Germany

Correspondence: B. Lauster (b.lauster@mpic.de)

Abstract. In urban areas, road traffic is a dominant source of nitrogen oxides ($\text{NO}_x = \text{NO} + \text{NO}_2$). Although the emissions from individual vehicles are regulated by the European emission standards, real driving emissions often exceed these limits. In this study, two MAX-DOAS instruments on opposite sides of the motorway were used to measure the NO_2 absorption caused by road traffic at the A60 motorway close to Mainz, Germany. In combination with wind data, the total NO_x emissions for the occurring traffic volume can be estimated. We show that the measured emissions exceed the maximum expected emissions calculated from the European emission standards by a factor of 11 ± 7 . One major advantage of the method used here is that from MAX-DOAS measurements the integrated NO_2 concentration over the lowermost 2 to 3 km is determined. Thus, all emitted NO_2 molecules are detected independent from their altitude and therefore the whole emission plume originating from the nearby motorway is captured by these measurements which is a key advantage compared to other approaches such as in-situ measurements.

1 Introduction

Nitrogen oxides (NO_x) is a collective term for nitrogen dioxide (NO_2) and nitric oxide (NO). In the troposphere, a photochemical reaction with ozone leads to an equilibrium state between NO_2 and NO (Pandis and Seinfeld, 2006). A large fraction of the global emissions of NO_x originates from anthropogenic sources. Therefore, nitrogen oxides do not only play a major role in atmospheric chemistry but are also important in terms of air quality. The World Health Organization reports negative short-term as well as long-term exposure effects in pulmonary function and in other organs (World Health Organization et al., 2000). For this reason, the limitation of the concentration of nitrogen oxides is part of the European programme regarding ambient air quality and cleaner air (European Parliament and Council of the European Union, 2008).

Fossil fuel combustion from road traffic is a major contributor to NO_x emissions. Hence, the European emission standards were introduced to regulate the exhaust emissions of new vehicles in the EU since 1998 (European Parliament and Council of the European Union, 1998) and tightened in 2007 by a new regulation bringing into force the so-called Euro 5 and Euro 6 norms (European Parliament and Council of the European Union, 2007). New vehicles sold in the EU need to undergo a type-approval procedure which verifies the compliance with these regulations. This procedure is standardised by the New European



Driving Cycle (NEDC) and includes the measurement of exhaust emissions on a chassis dynamometer (European Parliament and Council of the European Union, 1970).

However, various studies (Carslaw et al., 2011; Chen and Borcken-Kleefeld, 2014) have shown that the real driving conditions are more dynamic than the tested driving cycles. In addition, it is known that several manufacturers have installed software that manipulates the test results by reducing emissions specifically during the test procedure (Borgeest, 2017). This results in increased exhaust emissions during normal driving operation.

In-situ measurements such as used in vehicle chasing experiments, e.g. performed by Pöhler and Engel (2019), need to convert NO into NO₂ as they directly measure the exhaust plume. Furthermore, this approach is dependent on the exact position of the emission source and the inlet of the measuring instrument. Others use remote sensing techniques (Carslaw et al., 2011; Chen and Borcken-Kleefeld, 2014) to measure exhaust gases across-road. However, these require an estimate of the amount of primary NO₂ in the exhaust. Hence, the retrieval of the total amount of emitted NO_x is afflicted with large errors. Moreover, the across-road method can only give a point measurement and is not necessarily representative for the average emission of a vehicle. Both approaches are able to resolve the emission of individual vehicles but are depending on the wind field and the position of the exhaust pipe with respect to the measuring instrument.

Nevertheless, in the atmosphere NO and NO₂ form an equilibrium state which is mainly influenced by the ozone concentration and solar irradiance but not the primary composition and amount of the exhaust gases. Thus, the Multi AXis Differential Optical Absorption Spectroscopy (MAX-DOAS) yields a key advantage when operated at some distance from the emission source. The method is described in more detail in the next section.

2 Method

The MAX-DOAS method (Platt and Stutz, 2008) allows measuring the differential slant column density (DSCD) of different trace gases (Hönninger et al., 2004). Hereto, spectra of scattered sunlight are recorded at different elevation angles using ground based instruments. To convert the slant column density (SCD), which represents the integrated concentration along the slant light path, into the vertical column density (VCD), the so-called air mass factor (AMF) is needed. For trace gas layers close to the ground the geometric approximation for the AMF can be used (Hönninger et al., 2004). The integrated trace gas concentration along the vertical path is then given by

$$\text{VCD} = \frac{\text{SCD}}{\text{AMF}} \approx \sin(\alpha) \cdot \text{SCD} \quad (1)$$

where α is the elevation angle.

In order to remove the Fraunhofer lines, the logarithm of a so-called Fraunhofer reference spectrum with preferably minimal trace gas absorption is subtracted from the logarithm of the measured spectra. To fulfil this criterion, the reference spectrum is usually recorded with an elevation angle $\alpha = 90^\circ$, i.e. in zenith direction. Assuming that for a given solar zenith angle the stratospheric absorption is constant for measurements at different elevation angles, the differential SCD yields the integrated tropospheric concentration of a specific trace gas (for an altitude range from the surface up to about 2 to 3 km, Frieß et al., 2019, and references therein).



In this study, the MAX-DOAS method is used to measure the NO_2 emissions of vehicles on a motorway. Using two MAX-DOAS instruments, the background NO_2 DSCD is subtracted from the total NO_2 DSCD and thus yields the NO_2 SCD caused by the traffic emissions. In a final step, the derived NO_2 SCD is converted into the NO_x emissions by combining it with wind data and assuming a steady state NO_x to NO_2 ratio. These steps are described in detail below.

2.1 Experimental setup

To retrieve the amount of NO_x emitted by road traffic, two Tube MAX-DOAS instruments (Donner, 2016) were set up on both sides of a motorway. With these instruments, it is possible to measure the NO_2 DSCD of the ambient air along the viewing direction. The chosen measurement site is located along the heavily used A60 motorway close to Mainz, Germany, and has a long straight section which provides an advantageous geometry for the measurement setup. The exact alignment of the instruments for the presented measurement day is depicted in Fig. 1 and shows that the viewing direction is northward and parallel to the lane of traffic. On the measurement day, continuous westerly wind was present so that the air mass transport was perpendicular to the motorway as well as to the viewing direction of the instruments. From the difference between the upwind (west side) and downwind (east side) signals, the emissions of the motorway are estimated. The locations of the instruments were about 160 m and 220 m to the west and east side of the motorway, respectively. Therefore, the area enclosed by the two Tube MAX-DOAS instruments contains the motorway section and a railway track. Possible sources of NO_x are thus traffic emissions from cars, trucks and trains.

Measurements were taken at an elevation angle of 20° and with a total integration time of 2 s. The short integration time favours a high temporal resolution even if the quality of the spectral fit (Sect. 2.2) decreases slightly at the same time. The choice of a rather high elevation angle constrains not only the sensitivity region but also decreases the influence of variations in the background signal by reducing the light path length in the lowermost atmosphere. It should be noted that there were broken clouds on the measurement day which possibly induce differences between the two instruments. This effect is further analysed in Sect. 2.3.

In addition, a camera and a weather station were positioned on the upwind side to obtain further information. Taking videos with this setup makes it possible to observe the traffic density on the motorway. The weather station records the wind direction and wind velocity as well as several other meteorological parameters such as pressure and temperature every second.

2.2 Spectral analysis

The spectral analysis of the obtained spectra is performed using the QDOAS software (version 2.112.2, Danckaert et al., 2012). As a reference, a series of 90° measurements were taken simultaneously with both Tube MAX-DOAS instruments at the upwind measurement site. In order to categorise differences between the two instruments (Sect. 2.3), the reference measurements were taken at the same location after the measurement series was completed on both sides of the motorway. The wavelength calibration is accomplished using a high resolution solar spectrum (Chance and Kurucz, 2010). For the analysis, a wavelength range of 400 nm to 460 nm was selected. The DOAS fit includes trace gas absorption cross-sections (NO_2 at 298 K (Vandaele et al., 1998), O_4 at 293 K (Thalman and Volkamer, 2013), O_3 at 223 K (Serdyuchenko et al., 2014), and H_2O



90 (Rothman et al., 2010)) as well as two ring spectra, calculated with DOASIS (Kraus, 2003) using the reference spectrum, and a polynomial of 5th order also allowing an intensity offset. The spectral analysis is run separately for each instrument yielding the NO₂ DSCD time series for both measurement sites.

2.3 Instrumental differences

To estimate the influence of instrumental differences between the two Tube MAX-DOAS instruments on the NO₂ results, the 95 reference spectra are investigated in more detail. These measurements were taken simultaneously with both instruments on the upwind side with an elevation angle of 90° (zenith view). Fig. 2 shows the time series of the NO₂ results for these spectra. The first 90° measurement of each instrument is taken as a reference.

As can be seen, in the grey shaded area the standard deviation between the measurements of the two instruments only amounts to

$$100 \quad \Delta(\text{NO}_2 \text{ DSCD}) = 0.4 \times 10^{14} \text{ molec cm}^{-2} \quad (2)$$

whereas for the spectra after 15:05 UTC the signal differs widely with a standard deviation of $7.9 \times 10^{14} \text{ molec cm}^{-2}$. This increased deviation is due to clouds passing by (see Sect. A1). Thus, the measurements in the grey shaded area show that both instruments measure similar NO₂ DSCDs for the same measurement conditions, i.e. the same setup, viewing direction and cloud conditions. Therefore, these spectra are being integrated to minimise noise and used as fixed references which assures 105 that both instruments are analysed under the same conditions.

2.4 Integration time

In order to investigate the influence of the integration time on the spectral analysis, the fitting procedure is performed for spectra with different integration times but the same fit settings. Therefore, two or more spectra are added before performing the DOAS fit. The result of the NO₂ retrieval as well as the average root mean square (RMS) over each measurement series is 110 depicted in Fig. 3. The standard error of the average NO₂ DSCD is about $0.006 \times 10^{16} \text{ molec cm}^{-2}$ and thus not visible in the Figure. The average NO₂ error, which is given by the QDOAS analysis, shows the same trend as the average RMS. Although the average RMS decreases for longer integration times, the NO₂ retrieval yields the same result regardless of the integration time. The standard deviation between the results for different integration times amounts to less than $8 \times 10^{12} \text{ molec cm}^{-2}$ for the east side and $10 \times 10^{12} \text{ molec cm}^{-2}$ for the west side measurements which is three orders of magnitude smaller than the 115 NO₂ signal. Consequently, the measurements taken with an integration time of 2 s give sufficient results above the detection limit which is preferable as high temporal resolution is necessary to resolve specific traffic events.



3 Results

3.1 Measurement results

120 The measurement results for the 10 May 2019 are shown in Fig. 4 in panel (A) to (E). Panel (A) depicts the time series of the measured NO_2 DSCDs for both, the upwind and downwind side, analysed as described in Sect. 2.2. The next panel (B) shows the difference between both signals

$$\text{SCD}_{\text{traffic}} = \text{DSCD}_{\text{downwind}} - \text{DSCD}_{\text{upwind}}. \quad (3)$$

A persistent offset is found with a mean value of

125
$$\overline{\text{SCD}}_{\text{traffic}} = (0.185 \pm 0.009) \times 10^{16} \text{ molec cm}^{-2} \quad (4)$$

as represented by the orange line. The error is calculated using the error propagation of the standard errors of the mean for both instruments and additionally includes the deviation $\Delta(\text{NO}_2 \text{ DSCD})$ between both instruments as derived in Sect. 2.3.

As there are no large sources of NO_2 other than the motorway close to the measurement site, the background NO_2 DSCDs in both measurements can be assumed to be the same. Therefore, the difference between both sides is most likely due to traffic
130 emissions. There seems to be no significant additional emission due to the passing trains (marked by the dashed grey lines in the Figure) although the railway next to the measurement site is only used by diesel trains. Temporal variations can be found in the derived difference in addition to the constant offset. However, clouds have only a small impact on the measurement result as discussed in Sect. A2. Panel (C) depicts the amount of traffic observed during the measurement period for which the number of vehicles was counted over one-minute intervals on a sample basis using the recorded videos. (D) and (E) present
135 the wind data measured by the weather station. It shows the wind direction and the wind velocity at the upwind side. For the wind velocity, also the minimum and maximum values over 1 s using a sampling rate of 4 Hz are depicted in grey.

3.2 Plume age

For a better understanding of the retrieved signal, the wind field needs further investigation. The quantity of interest is the wind velocity $v_{\text{wind},\perp}$ perpendicular to the viewing direction of the Tube MAX-DOAS instruments whose viewing directions
140 are assumed to be parallel to the motorway. Thereby, the age of the measured plume can be quantified which is needed to retrieve the total emission (Sect. 3.3). The perpendicular wind velocity $v_{\text{wind},\perp}$ is shown in Fig. 4 (F) and is calculated using the measured wind velocity and the wind direction. From the alignment of the two Tube MAX-DOAS instruments as depicted in Fig. 1, it can be seen that the viewing direction corresponds to approx. 330° . The perpendicular wind velocity is thus

$$v_{\text{wind},\perp} = v_{\text{wind}} \cdot \cos(\phi_{\text{wind}}) \quad (5)$$

145 with

$$\phi_{\text{wind}} = \phi_{\text{wind,meas}} - 330^\circ + 90^\circ, \quad (6)$$



where $\phi_{\text{wind, meas}}$ is the measured wind direction at the weather station. The error can be calculated using the propagation of uncertainty principle and taking into account the minimum and maximum values of the wind data. An additional error for a possible misalignment of the weather station with regard to the viewing direction of the telescopes of 2° is considered. During the measurement period, the wind velocity perpendicular to the viewing direction is on average

$$\bar{v}_{\text{wind}, \perp} = (2.8 \pm 1.0) \text{ m s}^{-1}. \quad (7)$$

Taking into account the average distance between the motorway and the downwind instrument's viewing direction $x = (195 \pm 25) \text{ m}$ estimated from Fig. 1 within the main area of high sensitivity, an average age of an air parcel of

$$t = (1.2 \pm 0.4) \text{ min} \quad (8)$$

can be obtained. However, variations in the wind velocity and wind direction on short time scales affect the transport of an air parcel. Therefore, the plume age cannot always be correctly represented by Eq. 8. The correlation between the wind field and the measured NO_2 SCDs is further discussed in Sect. A3.

3.3 Estimation of real driving emissions

To estimate the real driving emissions, first the mean NO_2 SCD must be converted into a VCD using the geometric approximation as given in Eq. 1. Thus, for the elevation angle of $20 \pm 2^\circ$, the measurement yields

$$\overline{\text{VCD}}_{\text{traffic}} = (0.63 \pm 0.07) \times 10^{19} \text{ molec m}^{-2}. \quad (9)$$

Multiplying this value by the average wind velocity perpendicular to the viewing direction, the measured emission of NO_2 amounts to

$$E_{\text{meas}, \text{NO}_2} = (1.8 \pm 0.7) \times 10^{19} \text{ molec (m s)}^{-1}. \quad (10)$$

This value now describes the number of molecules emitted per meter and second along the motorway section. It is a direct quantity of the measurements and can be converted into emissions per vehicle per second by dividing by the number of vehicles per length of the motorway.

In combustion processes, N_2 is mainly oxidised into NO and in the atmosphere it is further oxidised into NO_2 and other oxides of nitrogen (Pandis and Seinfeld, 2006) forming an equilibrium between NO and NO_2 . Therefore, to retrieve the total NO_x emissions from the observed NO_2 levels, the share of NO_2 in total NO_x has to be known.

In order to estimate the rate of NO to NO_2 conversion, we used the CAABA box-model simulation with representative environment conditions and a road traffic source for the measurement period. CAABA uses the atmospheric chemistry model MECCA that includes the state of the art chemical mechanisms (Sander et al., 2019). A fraction of the traffic-emitted NO is photochemically equilibrated with air NO_2 at the daytime near-surface conditions. We estimate that about two-thirds of the emitted NO is thus converted into NO_2 in about 4 min. After 2 min, about 90% of the traffic-emitted NO is converted into the observed NO_2 enhancement. One important factor regarding the conversion is the ambient ozone level, as it regulates the



photochemical NO_x cycling and influences the resulting NO_2 to NO repartitioning dynamics. However, our simulations with CAABA confirm that for the presented measurement the NO_2 to NO ratio is rather stable and yields a ratio of 0.7 ± 0.4 for the time $t = (1.2 \pm 0.4)$ min which was estimated above. That is due to sufficiently high ambient ozone concentrations which were measured at local environmental monitoring stations (42 ppb to 44 ppb, Mainz-Mombach, distance to the measurement site approx. 5 km, and Wiesbaden-Süd, approx. 9 km, Umweltbundesamt, 2019).

The corresponding NO_x to NO_2 conversion factor, for the time $t = (1.2 \pm 0.4)$ min an air parcel needs to get from the vehicle exhaust to the sensitivity region of the Tube MAX-DOAS instrument, can be deduced to be $f = 2.4 \pm 1.0$. The NO_x emission is then derived using

$$E_{\text{meas, NO}_x} = f \cdot E_{\text{meas, NO}_2} \quad (11)$$

which equals

$$E_{\text{meas, NO}_x} = (4.3 \pm 2.5) \times 10^{19} \text{ molec (m s)}^{-1}. \quad (12)$$

In case the equilibrium is already reached, a conversion factor of $f_{\text{eq}} = 1.5$ needs to be applied instead. Then, the total NO_x emission would amount to

$$E_{\text{meas, NO}_x, \text{eq}} = (2.7 \pm 1.1) \times 10^{19} \text{ molec (m s)}^{-1}. \quad (13)$$

The determination of the conversion factor f relies on the rather rough estimate of the age of the air parcel as well as the ozone concentration and chemical processes during the measurement period. Therefore, the equilibrium value gives an estimate which is independent of these factors. However, it can be seen that this is within the error of $E_{\text{meas, NO}_x}$. In the following, the more realistic value of $E_{\text{meas, NO}_x}$ will be taken for the comparison with the expected traffic emissions.

3.4 Expected traffic emissions and comparison to real driving emissions

To calculate the expected traffic emissions, the emission per vehicle needs to be computed. The limiting values for NO_x emissions, as given by the European emission standards, are summarised in Table 1. The limiting values for passenger cars are given in NO_2 equivalents per km depending on the fuel type. For trucks, the values are reported in NO_2 equivalents per kWh. To undertake the following calculation, these emission standards need to be converted into limiting values per km. Therefore, the values are multiplied by a conversion factor of $1.5 \pm 0.5 \text{ kWh l}^{-1}$. This is composed of the fuel value 10.4 kWh l^{-1} of diesel fuel, the efficiency of a diesel engine of about 40 % and an average consumption for trucks of 36 l per 100 km (Hilgers, 2016). The error accounts for varying fuel consumption of ± 10 l per 100 km and the uncertainty in the efficiency of the vehicle engine.

For the calculations, the statistical composition of the vehicle fleet is considered (see Table 2). The passenger car fleet is broken down by registration districts, fuel types and emission groups. To analyse the emission per vehicle, the statistical distribution of Rheinhessen-Pfalz is chosen. This also includes the city of Mainz and the Mainz-Bingen region. Note that in this area more cars with old emission standards (Euro 3 and 4) are registered compared to the average in Germany. The



relative number of trucks is broken down by emission group only and relates to the distance travelled by German trucks. Attention should be paid to the fact that non-German trucks account for about 35 % of the total distance travelled in Germany
210 (Kraftfahrt-Bundesamt, 2017).

From the emission standards and the statistical composition of the vehicle fleet, the expected emission per vehicle can be calculated. The weighted average of the emission limits amount to

$$E_{\text{limit, cars}} = (116 \pm 5) \text{ mg km}^{-1} \quad (14)$$

and

$$215 \quad E_{\text{limit, trucks}} = (1248 \pm 277) \text{ mg km}^{-1} \quad (15)$$

for passenger cars and trucks, respectively. The observed amount of traffic is deduced by counting the vehicles as shown in Fig. 4 and shows average values of

$$N_{\text{cars}} = (91 \pm 4) \text{ min}^{-1} \quad (16)$$

and

$$220 \quad N_{\text{trucks}} = (6 \pm 2) \text{ min}^{-1}. \quad (17)$$

The error estimation accounts for miscounting the number of vehicles on the video e.g. when a truck shields the view of the other traffic lanes. Taking into account the average traffic volume, the expected total emission for the measuring period is given by

$$E_{\text{calc, NO}_x} = N_{\text{cars}} \cdot E_{\text{limit, cars}} + N_{\text{trucks}} \cdot E_{\text{limit, trucks}} \quad (18)$$

225 which yields

$$E_{\text{calc, NO}_x} = (0.39 \pm 0.07) \times 10^{19} \text{ molec (m s)}^{-1}. \quad (19)$$

Here, it is used that the NO_x emissions are given in NO_2 equivalents and thus 1 mg of NO_x emissions correspond to 1.3×10^{19} molec.

The expected emissions calculated from the European emission standards can now be compared to the measured NO_x
230 emissions. Evidently, the measured amount of NO_x is by a factor 11 ± 7 larger than expected. Even if an equilibrium state between NO and NO_2 for the measured traffic emissions was assumed, the measured NO_x emissions still show a higher value (by a factor of 7 ± 3) compared to the calculated emissions. Moreover, in the very unlikely case that the exhaust gases primarily consist of NO_2 and the measured NO_2 difference directly equals the NO_x emissions, this discrepancy remains unexplained. Possible error sources in the measurement cannot completely explain these differences.

235 As the traffic volume was relatively constant throughout the measurement period, it is more likely that the statistics do not reflect the vehicle fleet well enough and/or a large part of the vehicles does not meet the emission standards. Here, it should be noted that the deviations of the actual vehicle composition from the assumed one cannot be the sole reason for this factor.



Assuming that only Euro 3 diesel cars and Euro III trucks, i.e. the technical status quo of the year 2000, were driving during the measurement period, the expected traffic emission would amount to

$$E_{\text{calc, NO}_x, \text{Euro3/III}} = (2.0 \pm 0.5) \times 10^{19} \text{ molec (m s)}^{-1} \quad (20)$$

which is still lower than the measured emission. As today only a minor fraction of all vehicles is registered as Euro 3 cars and Euro III trucks, this worst case scenario is highly unlikely. Considering that especially non-German trucks more often drive with defective exhaust gas systems, these could lead to large emissions even exceeding the Euro III norm. Thereby, the discrepancy between the expected and measured emissions could be partly explained. However, trucks only account for a small amount of the total traffic volume. This again implies an excess of the European emission standards regarding NO_x emissions also for a significant number of passenger cars.

4 Conclusions

The measurement of NO_x emissions at the A60 motorway close to Mainz, Germany, gives an estimate of the real driving emissions. With two MAX-DOAS instruments set up on both sides of the motorway, it is possible to retrieve the NO₂ signal caused by the road traffic and calculate the total NO_x emissions for the occurring traffic volume.

The most uncertain aspect during the analysis of the data was the age of the measured plume at the downwind side. It directly affects the conversion factor f of the NO_x to NO₂ ratio and thus the final result of the measured emission (Eq. 11). To further investigate the effect of the plume age, it is favourable to set up several MAX-DOAS instruments downwind with different distances to the motorway. Thereby, the setup of the instruments could be optimised and the equilibrium state of NO₂ for the given weather conditions can be measured. This yields a more accurate conversion factor.

Other aspects such as the high ozone concentration and relatively constant wind are uncritical for the presented measurement day and allow to apply a constant conversion factor f to the average emission. Although the changing cloud cover caused large fluctuations in the NO₂ DSCDs, filtering the data leads to only slightly lower emissions. Consequently, this effect cannot explain the difference between the measured and expected emissions.

The main possible error source regarding the derivation of the expected NO_x emissions is the difference from the assumed vehicle fleet to the measured vehicle fleet. Although the statistics are relevant to the Mainz region, the exact composition remains unknown. However, the worst case calculation showed that the uncertainty of the vehicle fleet cannot explain the deviation from the measured emission. Presumably, a considerable amount of vehicles did not meet the European emission standards. Moreover, it must be assumed that a substantial number of trucks are non-German vehicles. Recent studies showed that a large fraction of these vehicles had conspicuously high emissions which indicate deactivated fuel cleaning units (Pöhler and Engel, 2019). These could also explain the temporal variations in the measured time series. Applying this method at different measurement sites, different driving conditions (e.g. the slope of the motorway section, the allowed speed limit, road works etc.) and the impact of the composition of the vehicle fleet could be investigated in more detail.

It can be concluded that the measured emissions exceed the maximum expected emissions calculated from the European emission standards (Umweltbundesamt) by a factor of 11 ± 7 . This observation is in line with the work of other groups (Carslaw



et al., 2011; Chen and Borcken-Kleefeld, 2014; Pöhler and Engel, 2019). Especially, the whole plume originating from the nearby motorway was measured rather than individual vehicle plumes and hence the possibility that parts of the plume get overlooked can be neglected which is a key advantage compared to other approaches such as in-situ measurements.

Data availability. Measurement data are provided in the supplement.

275 Appendix A

A1 Effect of clouds on the reference spectra

Clouds can have a great impact on MAX-DOAS measurements. A change of the light path is caused by the increased scattering probability in clouds as there are more particles compared to the ambient air. Furthermore, the wavelength dependency of the scattered light changes for particle scattering processes compared to pure Rayleigh scattering. This effect already occurs for aerosols and is even more pronounced for clouds.

There are different methods to identify and classify clouds. Here, the temporal variation of the colour index (Wagner et al., 2014) is used. The colour index (CI) is defined as the ratio of two radiance values at different wavelengths. In this case, the wavelengths 320 nm and 440 nm are chosen. Thereby, the wavelengths cover a large range to pronounce the effect of the wavelength dependency.

The CI is calculated for the 90° measurements as shown in Fig. 2 and the obtained temporal evolution is given in Fig. A1. As for cloud free conditions a constant CI is expected, it can be seen that measurements after 15:05 UTC were affected by clouds. This leads to larger deviations in the retrieved NO₂ signal as shown in Sect. 2.3. Accordingly, the CI analysis also encourages the approach to use only the 90° measurements in the grey shaded area as a reference.

A2 Effect of clouds on the measurement result

Calculating the CI as described in Sect. A1 for all spectra, a characteristic behaviour can be seen (Fig. A2). As high temporal variation indicates cloud cover, all spectra where the CI is below the reference CI_{ref} are filtered. The reference was inferred by fitting a 2nd order polynomial to the data. The filtered time series are displayed in Fig. A3 where the dashed line indicates the filter threshold. Recalculating the mean difference between the two measurement sites yields

$$\overline{\text{SCD}}_{\text{traffic, filtered}} = (0.156 \pm 0.005) \times 10^{16} \text{ molec cm}^{-2} \quad (\text{A1})$$

which is about 16 % smaller compared to the unfiltered case.

A3 Correlation to the wind field

Assuming a constant emission, the NO₂ difference is expected to be reciprocal to the wind velocity. However, an air parcel is also affected by obstacles such as trees and follows the turbulent flow of air. Furthermore, the wind varies on time scales of



less than 1 min whereas the transport of the air parcel from the emission location to the sensitivity region of the MAX-DOAS
300 instrument happens on larger time scales of 1 min or more. This means that the time of the wind measurement and the time
of the NO₂ measurement are shifted by a time difference in which the wind might change strongly. Hence, the age of the air
parcel cannot always be correctly represented by the simple calculation in Eq. 8. In Fig. A4 the traffic emission SCD_{traffic} is
plotted against the inverse of the wind velocity $v_{\text{wind},\perp}^{-1}$ showing no correlation ($R^2 = 0.001 \ll 1$) between the two quantities.

To further test this hypothesis, both - the wind measurements and the time series of the NO₂ differences - are averaged
305 over a time period of 12 min. Figure A5 shows a higher correlation between both quantities ($R^2 = 0.365$). The data points
are fitted using the linear least squares method (LLS, orange line) as well as using the orthogonal distance regression (ODR,
green line). Here, ODR is able to take into account the standard errors of the mean values in the fitting procedure (Cantrell,
2008). In doing so, the slope of the fit increases and at the same time the intercept decreases. Comparing the fit results with
the obtained emission $E_{\text{meas, NO}_2}$ over the complete NO₂ measurement series as described in Sect. 3.3, a slope of about
310 $5000 \pm 2000 \text{ molec (m s)}^{-1}$ is expected. The fits from Figure A5 show slopes of $4230 \pm 208 \text{ molec (m s)}^{-1}$ for the LLS and
 $7539 \pm 2013 \text{ molec (m s)}^{-1}$ for the ODR method which are in agreement with the expected value.

Nevertheless, the weak correlation is not completely surprising because of the low variability of the wind velocity. Moreover,
a constant wind velocity is generally advantageous for the measurements.

Author contributions. TW, SDÖ and BL designed the experiment. Adaptation of the instruments to the measurement setup was implemented
315 by SDO, SDÖ and BL. SDÖ, BL and KU performed the measurements. SG developed and performed the simulations. BL prepared the
manuscript with contributions from all co-authors. TW, SB, SDÖ and SDO contributed with valuable feedback and supervised the study.

Competing interests. The authors declare that they have no conflicts of interests.

Acknowledgements. We acknowledge the electronics workshop (i.e. Thomas Klimach, Christian Gurk, Mark Lamneck and Frank Helleis)
and the mechanical workshop (i.e. Michael Dietrich and Ralf Wittkowski) of the Max-Planck Institute for Chemistry, Mainz, for the contin-
320 uous support in the development of the Tube MAX-DOAS instrument. We are also thankful to Denis Pöhler (Airyx GmbH) for sharing his
expertise on traffic emission estimation.



References

- Borgeest, K.: Manipulation von Abgaswerten: Technische, gesundheitliche, rechtliche und politische Hintergründe des Abgasskandals, Springer-Verlag, <https://doi.org/10.1007/978-3-658-17181-0>, 2017.
- 325 Cantrell, C. A.: Technical Note: Review of methods for linear least-squares fitting of data and application to atmospheric chemistry problems, *Atmospheric Chemistry and Physics*, 8, 5477–5487, <https://doi.org/10.5194/acp-8-5477-2008>, 2008.
- Carslaw, D. C., Beevers, S. D., Tate, J. E., Westmoreland, E. J., and Williams, M. L.: Recent evidence concerning higher NO_x emissions from passenger cars and light duty vehicles, *Atmospheric Environment*, 45, 7053–7063, <https://doi.org/10.1016/j.atmosenv.2011.09.063>, 2011.
- 330 Chance, K. and Kurucz, R. L.: An improved high-resolution solar reference spectrum for earth's atmosphere measurements in the ultraviolet, visible, and near infrared, *Journal of quantitative spectroscopy and radiative transfer*, 111, 1289–1295, <https://doi.org/10.1016/j.jqsrt.2010.01.036>, 2010.
- Chen, Y. and Borcken-Kleefeld, J.: Real-driving emissions from cars and light commercial vehicles—Results from 13 years remote sensing at Zurich/CH, *Atmospheric Environment*, 88, 157–164, <https://doi.org/10.1016/j.atmosenv.2014.01.0400>, 2014.
- 335 Danckaert, T., Fayt, C., Van Roozendael, M., De Smedt, I., Letocart, V., Merlaud, A., and Pinardi, G.: QDOAS Software user manual, 2012.
- Donner, S.: Mobile MAX-DOAS measurements of the tropospheric formaldehyde column in the Rhein-Main region, Master's thesis, University of Mainz, <http://hdl.handle.net/11858/00-001M-0000-002C-EB17-2>, 2016.
- European Parliament and Council of the European Union: 70/220/EEC of 20 March 1970 on the approximation of the laws of the Member States relating to measures to be taken against air pollution by gases from positive-ignition engines of motor vehicles, *OJ L*, 76, 1–22, 340 1970.
- European Parliament and Council of the European Union: 98/69/EC of the European Parliament and of the Council of 13 October 1998 relating to measures to be taken against air pollution by emissions from motor vehicles and amending Council Directive 70/220/EEC, *OJ L*, 350, 12, 1998.
- European Parliament and Council of the European Union: Regulation (EC) No 715/2007 of the European Parliament and of the Council of 345 20 June 2007 on type approval of motor vehicles with respect to emissions from light passenger and commercial vehicles (Euro 5 and Euro 6) and on access to vehicle repair and maintenance information., *OJ L*, 171, 1–16, 2007.
- European Parliament and Council of the European Union: Council Directive 2008/50/EC on ambient air and cleaner air for Europe, *OJ L*, 151, 1–44, 2008.
- Frieß, U., Beirle, S., Alvarado Bonilla, L., Bösch, T., Friedrich, M. M., Hendrick, F., Piders, A., Richter, A., van Roozendael, M., Rozanov, 350 V. V., Spinei, E., Tirpitz, J.-L., Vlemmix, T., Wagner, T., and Wang, Y.: Intercomparison of MAX-DOAS vertical profile retrieval algorithms: studies using synthetic data, *Atmospheric Measurement Techniques*, 12, 2155–2181, <https://doi.org/10.5194/amt-12-2155-2019>, 2019.
- © Google Earth Pro: Mainz, 49°58'55.48"N 8°12'34.81"E, eye altitude 4.98 km.
Google 2018, GeoBasis-DE/BKG 2009., 2018.
- 355 Hilgers, M.: Kraftstoffverbrauch und Verbrauchsoptimierung, Springer, <https://doi.org/10.1007/978-3-658-12751-00>, 2016.
- Hönninger, G., Friedeburg, C. v., and Platt, U.: Multi axis differential optical absorption spectroscopy (MAX-DOAS), *Atmospheric Chemistry and Physics*, 4, 231–254, <https://doi.org/10.5194/acp-4-231-20040>, 2004.



- Kraftfahrt-Bundesamt: Lastfahrten im Inlandsverkehr nach Hauptverkehrsbeziehungen mit europäischen Lastkraftfahrzeugen im Jahr 2017, https://www.kba.de/DE/Statistik/Kraftverkehr/europaeischerLastkraftfahrzeuge/Inlandsverkehr/inlandsverkehr_node.html, last accessed: 18.07.2019, 2017.
- 360 Kraftfahrt-Bundesamt: FZ 1 Bestand an Kraftfahrzeugen und Kraftfahrzeuganhängern nach Zulassungsbezirken, 1. Januar 2019, <https://www.kba.de>, last accessed: 26.02.2020, 2019a.
- Kraftfahrt-Bundesamt: VD 5 Verkehr deutscher Lastkraftfahrzeuge Gesamtverkehr März 2019, <https://www.kba.de>, last accessed: 19.02.2020, 2019b.
- 365 Kraus, S.: DOAS Intelligent System, institute of Environmental Physics, University of Heidelberg, Cooperation with Hoffmann Messtechnik GmbH, 2003.
- Pandis, S. N. and Seinfeld, J. H.: Atmospheric chemistry and physics: From air pollution to climate change, Wiley, 2006.
- Platt, U. and Stutz, J.: Differential Optical Absorption Spectroscopy: Principles and Applications, Springer Science & Business Media, 2008.
- Pöhler, D. and Engel, T.: Bestimmung von realen Lkw NO_x-Emissionen (Real Driving Emissions) und hohen Emittlern auf deutschen
370 Autobahnen, 2019.
- Rothman, L., Gordon, I., Barber, R., Dothe, H., Gamache, R., Goldman, A., Perevalov, V., Tashkun, S., and Tennyson, J.: HITEMP, the high-temperature molecular spectroscopic database, *Journal of Quantitative Spectroscopy and Radiative Transfer*, 111, 2139–2150, <https://doi.org/10.1016/j.jqsrt.2010.05.001>, 2010.
- Sander, R., Baumgaertner, A., Cabrera-Perez, D., Frank, F., Gromov, S., Groß, J.-U., Harder, H., Huijnen, V., Jöckel, P., Karydis, V. A.,
375 et al.: The community atmospheric chemistry box model CAABA/MECCA-4.0, *Geoscientific model development*, 12, 1365–1385, <https://doi.org/10.5194/gmd-12-1365-2019>, 2019.
- Serduchenko, A., Gorshchev, V., Weber, M., Chehade, W., and Burrows, J.: High spectral resolution ozone absorption cross-sections—Part 2: Temperature dependence, *Atmospheric Measurement Techniques*, 7, 625–636, <https://doi.org/10.5194/amt-7-625-2014>, 2014.
- Thalman, R. and Volkamer, R.: Temperature dependent absorption cross-sections of O₂–O₂ collision pairs between 340 and 630 nm and at
380 atmospherically relevant pressure, *Physical chemistry chemical physics*, 15, 15 371–15 381, <https://doi.org/10.1039/C3CP50968K>, 2013.
- Umweltbundesamt: Emissionsstandards, <https://www.umweltbundesamt.de/themen/verkehr-laerm/emissionsstandards>, last accessed: 06.07.2019.
- Umweltbundesamt: Aktuelle Luftdaten, Fachgebiet II 4.2, Beurteilung der Luftqualität, <https://www.umweltbundesamt.de/daten/luftbelastung/aktuelle-luftdaten>, ozone concentration of 10 May 2019 at Mainz-Mombach (DERP007) and Wiesbaden-Süd (DEHE022),
385 2019.
- Vandaele, A. C., Hermans, C., Simon, P. C., Carleer, M., Colin, R., Fally, S., Merienne, M.-F., Jenouvrier, A., and Coquart, B.: Measurements of the NO₂ absorption cross-section from 42 000 cm⁻¹ to 10 000 cm⁻¹ (238–1000 nm) at 220 K and 294 K, *Journal of Quantitative Spectroscopy and Radiative Transfer*, 59, 171–184, 1998.
- Wagner, T., Apituley, A., Beirle, S., Dörner, S., Friess, U., Remmers, J., and Shaiganfar, R.: Cloud detection and classification based on
390 MAX-DOAS observations, *Atmospheric Measurement Techniques*, 7, 1289–1320, <https://doi.org/10.5194/amt-7-1289-2014>, 2014.
- World Health Organization et al.: Air quality guidelines for Europe, 2000.

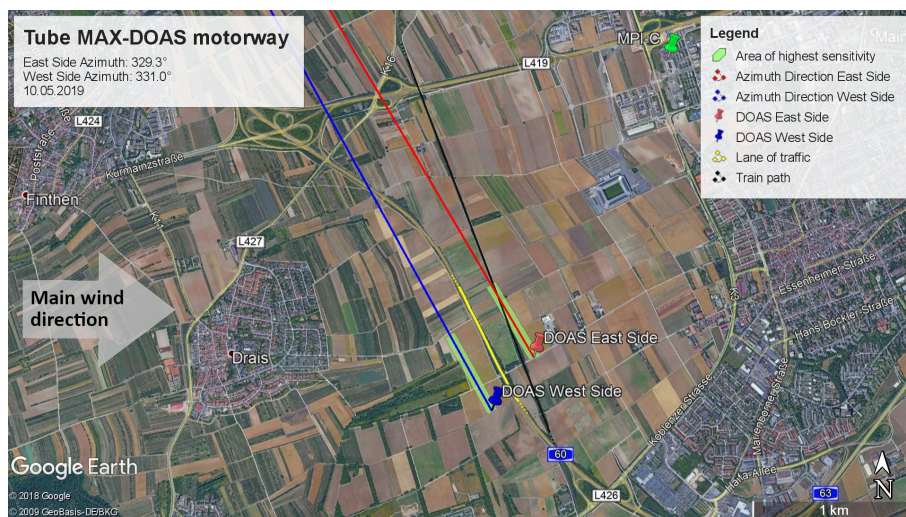


Figure 1. Alignment of the two Tube MAX-DOAS instruments on the measurement day, 10 May 2019. The instruments are located on both sides of the A60 motorway, Mainz, Germany, with a viewing direction parallel to the lane of traffic. The area between both instruments encloses the motorway and the railway track. On the measurement day, continuous wind from westerly directions was present. Created with © Google Earth Pro (2018).

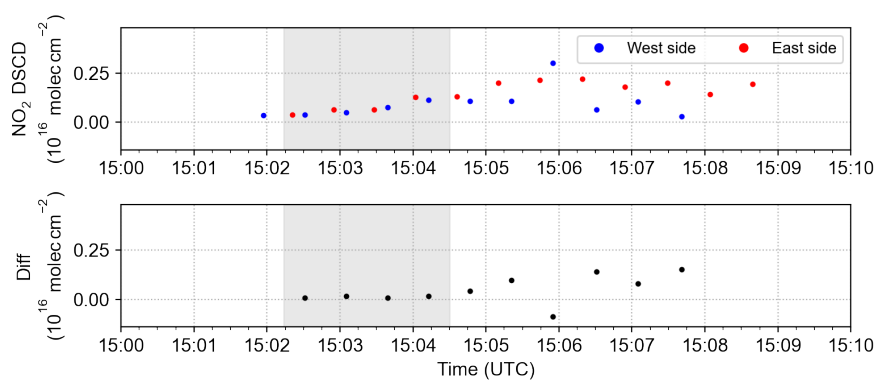


Figure 2. Time series of the NO₂ results for the 90° measurements of both instruments on the upwind side. In the upper panel the label refers to the place of each instrument during the measurement of the traffic emissions. The spectra are analysed using the first 90° spectrum as a reference. In the lower panel the difference between the two Tube MAX-DOAS instruments is depicted. The grey shaded area denotes the range where both measured similar NO₂ DSCDs.

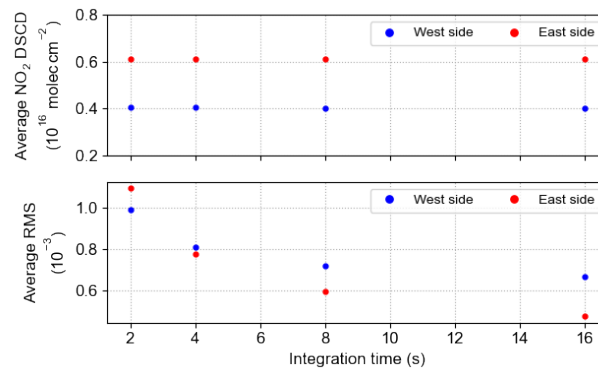


Figure 3. Average NO₂ DSCD and average RMS for both measurement sites (blue: west side, upwind; red: east side, downwind) for different integration times.

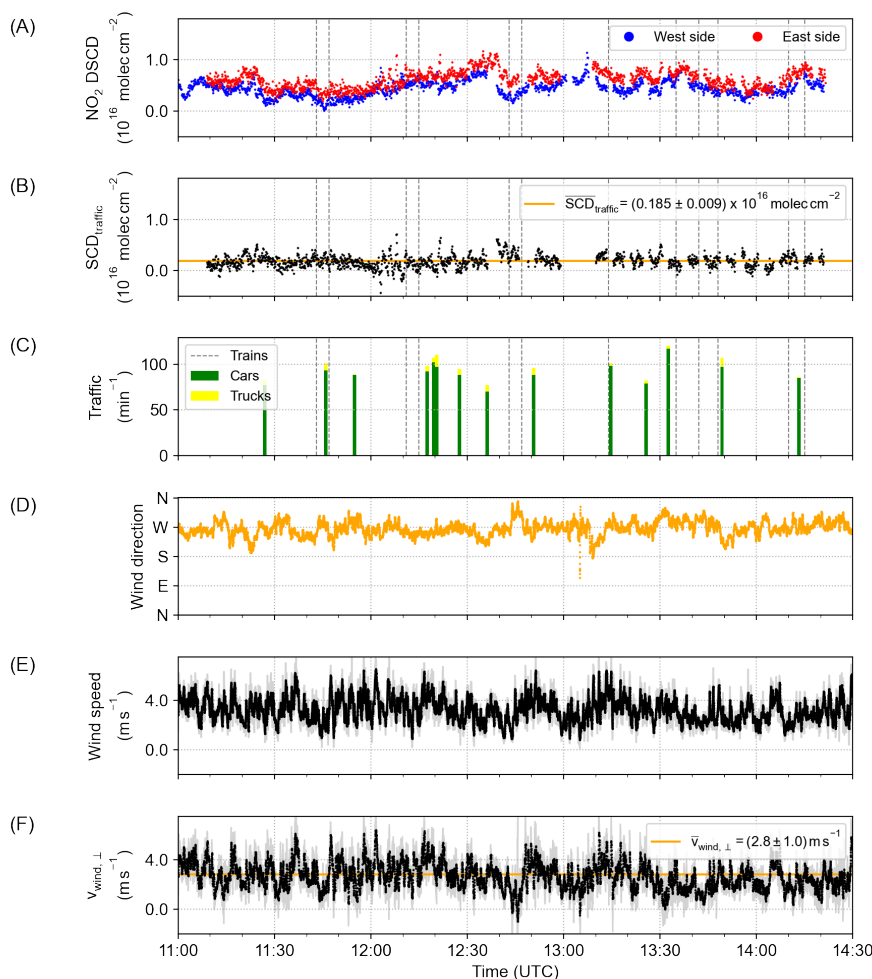


Figure 4. Time series of the measurement results of the 10 May 2019. (A) depicts the measured NO_2 DSCD for both measurement sites (blue: west side, upwind; red: east side, downwind). In (B) the difference $\text{SCD}_{\text{traffic}}$ between both signals is shown. The orange line symbolises the average value. (C) presents the traffic volume during the measuring duration. The number of vehicles was retrieved by counting from the videos over one-minute intervals on a sample basis. The dashed grey lines represent the times of passing trains. (D) and (E) depict the wind direction and wind velocity as measured by the weather station at the upwind side. The light grey values in (E) show the minimum and maximum wind velocities. (F) shows the wind velocity $v_{\text{wind},\perp}$ perpendicular to the viewing direction of the Tube MAX-DOAS instruments. The orange line denotes the mean value over the whole measurement period. Here, the light grey values depict the error $\Delta v_{\text{wind},\perp}$ of the calculated wind velocity.



Table 1. European emission standards for NO_x emissions (Umweltbundesamt).

For passenger cars separated into fuel types
in mg km⁻¹ NO₂:

| | Euro 3 | Euro 4 | Euro 5 | Euro 6 |
|--------|--------|--------|--------|--------|
| diesel | 500 | 250 | 180 | 80 |
| petrol | 150 | 80 | 60 | 60 |

For trucks in mg kWh⁻¹ NO₂:

| Euro III | Euro IV | Euro V | Euro VI |
|----------|---------|--------|---------|
| 5000 | 3500 | 2000 | 460 |



Table 2. Vehicle fleet composition by emission group in %.

| For passenger cars (Kraftfahrt-Bundesamt, 2019a): | | | | |
|---|--------|--------|--------|--------|
| | Euro 3 | Euro 4 | Euro 5 | Euro 6 |
| diesel | 3±1 | 6±1 | 11±1 | 8±1 |
| petrol | 6±1 | 23±1 | 16±1 | 16±1 |

| For trucks (Kraftfahrt-Bundesamt, 2019b): | | | | |
|---|----------|---------|--------|---------|
| | Euro III | Euro IV | Euro V | Euro VI |
| | 1±1 | 1±1 | 19±1 | 78±1 |

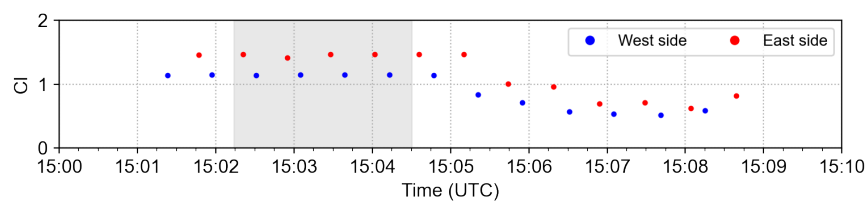


Figure A1. The temporal evolution of the colour index (CI) for the 90° measurements, which were taken simultaneously at the upwind side, is depicted. The label refers to the place of each instrument during the measurement of the traffic emissions. The grey shaded area depicts the range where both instruments measured the same NO₂ signal (compare to Fig. 2).

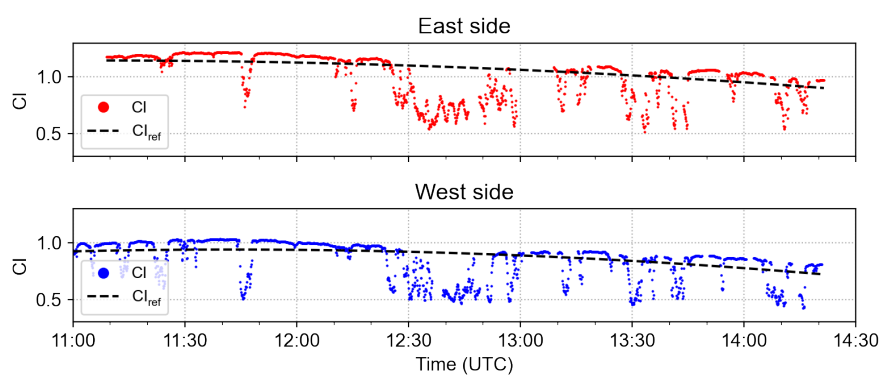


Figure A2. The colour index (CI) for both measurement series. The dashed line (CI_{ref}) indicates the filter threshold.

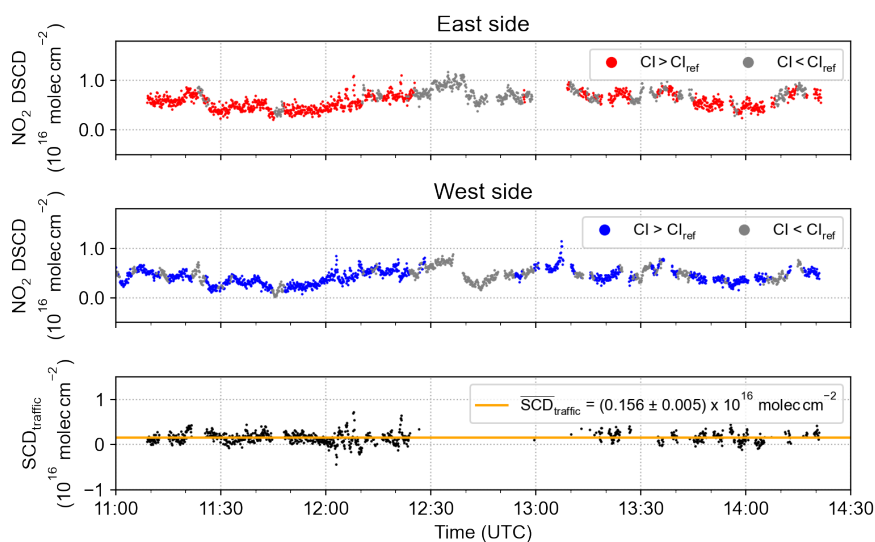


Figure A3. Analysis result of the NO_2 DSCDs for both sides (blue: west side, upwind; red: east side, downwind) with applied cloud filter based on the colour index (CI). The grey data points are filtered out. The resulting difference $\text{SCD}_{\text{traffic}}$ is depicted in the lowermost panel yielding slightly lower NO_2 SCDs compared to the unfiltered case.

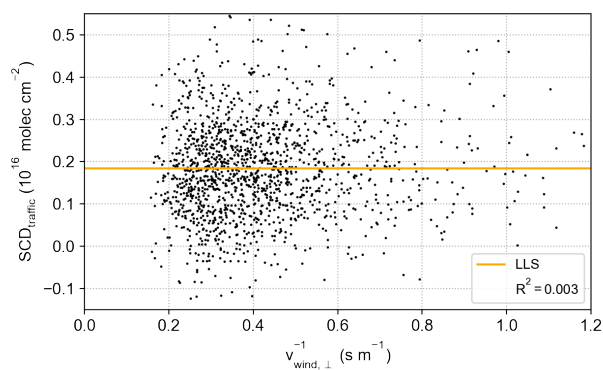


Figure A4. Correlation between the inverse of the wind velocity $v_{\text{wind},\perp}^{-1}$ perpendicular to the viewing direction of the Tube MAX-DOAS instruments and the NO_2 signal $\text{SCD}_{\text{traffic}}$ with a linear least squares (LLS) fit.

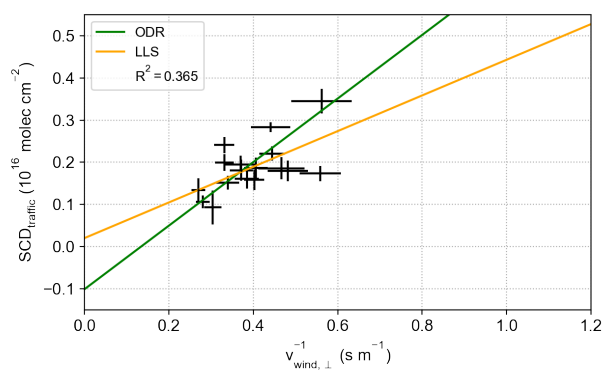


Figure A5. Correlation between the inverse of the wind velocity $v_{\text{wind},\perp}^{-1}$ perpendicular to the viewing direction of the Tube MAX-DOAS instruments and the NO_2 signal $\text{SCD}_{\text{traffic}}$ for a 12 min averaging time span. The data points were fitted using the linear least squares method (LLS) and orthogonal distance regression (ODR).